PHOTOMETRIC COMPOSITE FINGERPRINTS FOR RESIDENT SPACE OBJECTS

M. Kuhn(1), M . Michel(1), and T. Dekorsy(2)

(1)*Airbus Defence & Space, Germany, Email: moritz.kuhn@airbus.com*
(2)*DLR Institute for Technical Physics (ITP)*

ABSTRACT

Maintaining awareness of an increasingly crowded space environment poses the challenge of identifying different resident space objects (RSOs) and preventing mix-ups, in particular after a manoeuvre or period of non-observation, or for objects in close proximity to each other. This requires information about the objects in question beyond their orbital state, such as their attitude and rotation, shape and size, or surface reflective properties. While all of this information can in principle be reconstructed from light curve measurements, in practice this is often very challenging. On the other hand, simpler light curve features or object characteristics such as rotation period or colour index may not suffice to reliably identify RSOs.

We therefore propose a composite fingerprint comprising a combination of these less complex features, similar to browser fingerprinting techniques used to track non-cooperative internet users based on a combination of properties like their screen size or installed fonts.

In this paper, we selected a number of features and constructed fingerprints of over two thousand light curves, comprising roughly by equal parts simulated data and real RSO light curves recorded by the Airbus Robotic Telescope (ART). We then examined these fingerprints and their components regarding their uniqueness, stability and utility in RSO identification.

We find that even a simple fingerprint can support object identification in our dataset, though the method struggles with distinguishing very similar RSOs. We also find that these fingerprints are relatively stable over a timespan of weeks to months.

Keywords: Object Characterization; Light Curves.

1. INTRODUCTION

The space environment around the Earth is home to an ever-growing number of artificial satellites, contributing to scientific and economic advancements as well as military and intelligence-related endeavours. At the same time, the number of debris objects threatening the safe and sustainable utilization of this environment is also increasing. An observer or spacecraft operator wishing to maintain awareness of this complex domain is faced with the challenge of identifying different resident space objects (RSOs) and preventing mix-ups, so-called cross-tags and misidentifications. This is particularly relevant for objects that are tightly clustered after launch or after a debris-generating event; for objects performing rendezvous and proximity operations; or for objects recovered observationally after a significant length of time or after a manoeuvre.

Identification of these RSOs in similar orbits or after manoeuvres requires information about the object in question beyond its orbital state. While most RSOs are too small and too distant to allow resolved imaging by ground-based optical telescopes, these sensors can nonetheless contribute to RSO characterization via photometric measurements. Photometry and light curves encode a wealth of information about a RSO, including its attitude and rotation, shape and size, as well as surface reflective properties [1, 2, 3, 4]. However, while these properties could indeed facilitate identification, reconstructing an RSO's full attitude state or shape from light curve data is challenging even in the most favourable of cases [5, 6]. On the other hand, more easily obtained object characteristics such as rotation period, BVRI colour index or simple morphological properties of the light curve may not suffice to reliably identify RSOs.

To alleviate this issue, we propose a composite fingerprint comprised of a combination of these less complex properties. Similar to the browser fingerprinting techniques used by website operators and advertisers to track non-cooperative users on the internet, such a space object fingerprint aims to enable the identification of different space objects based only on information that is readily available.

There are several approaches to fingerprints for space objects besides the one described in this work: a method for using photometric data to prevent mistagging of RSOs has been presented in [7], using only the brightness data itself. An RSO fingerprint of a different kind is proposed in [8], an approach based on a single feature more similar to human biometric fingerprinting. In [6], a photometric fingerprint is constructed by multiple measurements of an

Proc. 9th European Conference on Space Debris, Bonn, Germany, 1–4 April 2025, published by the ESA Space Debris Office
Editors: S. Lemmens, T. Flohrer & F. Schmitz, (http://conference.sdo.esoc.esa.int, April 2025)

Feature	Definition
`angular_velocity`	Mean angular velocity during the measurement [arcsec/s]
`mean_mag`	Mean magnitude [mag]
`diff_means`	Absolute difference of the mean of the first and second half of the curve [mag]
`interpercentile_range`	Difference between the 95th and 5th magnitude percentile [mag]
`autocorrelation`	1-shift autocorrelation of the light curve [-]
`max_diff`	Maximum absolute difference of two neighbouring points [mag]
`frequency`	Strongest peak in Lomb-Scargle periodogram of the light curve [Hz]

Table 1: Features used to construct light curve fingerprints in this work.

object from different observation geometries, producing a fingerprint that is closely related to a Bi-direction Reflectance Function (BDRF). Similar work to this one is also done in [9].

The present paper is structured as follows: section 2 describes the concept of the RSO fingerprint and the fingerprint components selected for this work. Section 3 introduces the two sets of light curves used, one simulated and one real. Section 4 examines the performance of the fingerprinting as applied to our data. Section 5 provides a brief summary and outlines potential further steps.

2. SPACE OBJECT FINGERPRINTING

In theory, light curves of sufficient resolution in time and magnitude carry considerable information about the observed RSO, allowing recovery of its shape, surface reflective properties and full attitude state [10, 5, 1]. Obtaining these properties could also support an unambiguous RSO identification to prevent mistagging and mixups of RSOs, for tracklet-to-tracklet or catalogue correlation or to recover objects after manoeuvres or long periods without observation. In practice, however, the recovery of characteristics like an object's shape or full attitude state from photometric measurements is challenging at best, often requiring large amounts of observational data or additional information about the RSO [1]. For this reason, a more easily obtainable identification measure is desirable.

A comparable problem of keeping track of uncooperative individuals in a large population is encountered in web analytics and advertising. A growing number of privacy-conscious users disables or avoids cookies that would otherwise be used to identify them. Without these highly-identifiable properties, actors intending to track a browser or device use an eclectic collection of data such as screen resolutions, installed browser extensions or fonts to build a fingerprint [11]. This allows them to track all but the most privacy-minded users [12].

A similar approach seems to hold promise for RSO fingerprinting. We propose a composite fingerprint comprising features extracted or derived from passive optical light curves, potentially augmented by the inclusion of non-photometric data. While these features individually may be insufficient to distinguish between different RSOs in a population, they may be able to do so when taken together. Being derived from passive optical light curves, these features should ideally be able to be acquired with only a passive optical sensor, comprising a telescope or lens, camera and photometric filters. Additionally, they should also be intercomparable between different sensors, as long as the sensors are properly calibrated.

2.1. Fingerprint Components

Potential features to serve as fingerprint components include nearly any conceivable property of the light curve, such as its mean magnitude or any periodic variation that may be present. Work identifying such features has been done in the field of time-domain astronomy [13, 14].

The addition of non-photometric features, some of which – like an object's angular velocity on the sky – may be easily obtained in the course of a light curve measurement, may provide additional entropy. Other measurements such as an object's colour index, polarimetric or spectrometric data or orbital parameters likewise seem potentially useful, but require additional equipment or processing beyond a simple passive-optical telescope and camera. For that reason, these features are not considered further here.

The features chosen for this work are summarized in Tab. 1. They were selected to be as few, simple and interpretable as possible, drawing some inspiration from the light curve features described in [13]. Notably, the average angular velocity of an object during the light curve measurement was added as a non-photometric feature that is easily obtained alongside light curve data. Two features warrant additional brief discussion. The 1-shift autocorrelation, i.e. the correlation of the light curve to a copy of itself shifted by one measurement, acts as a measure of smoothness: it will be close to 1 for a smoothly varying light curve, 0 for one without an overall linear relation between each point and the one before and -1 for a curve in which high and low points tend to alternate, such as an undersampled light curve of a rotating object. The `frequency` feature in this work is defined as the location of the strongest peak in a Lomb-Scargle periodogram of the light curve [15]. However, we note that using only the strongest peak potentially loses additional information contained in weaker peaks, especially

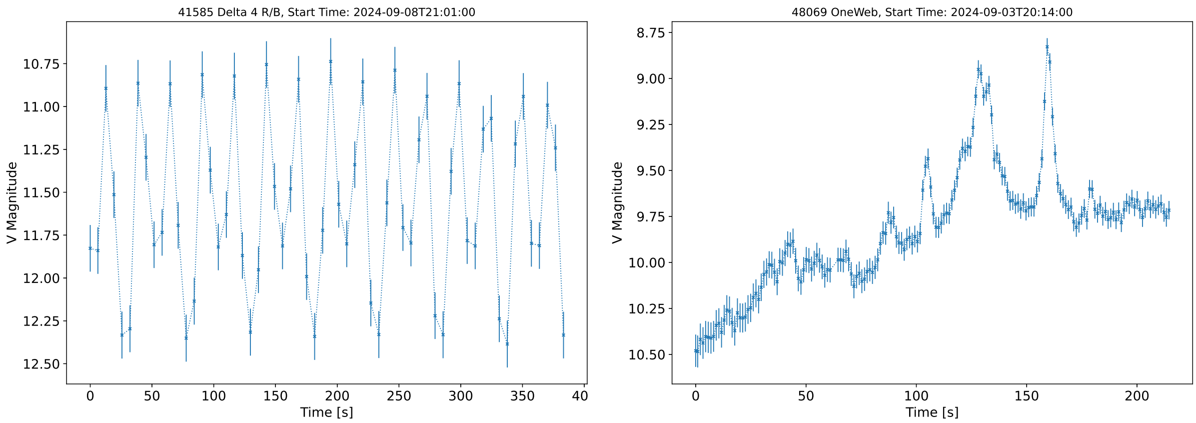

Figure 1: Light curves captured by ART in September 2024.

since most light curves of rotating objects are not simply sinusoids of a single frequency.

For ease of handling and based on the observations that the values of these features tend to fall within relatively few more or less distinct categories, we sort the feature values into a small number of bins and record the bin number. We set the bin boundaries based on domain knowledge and the inspection of a different set of observations that was not otherwise used in this work. This means that in the context of this work, a measurement's fingerprint is represented by a seven-element vector of small integers.

Finally, it is worth noting that despite the stated goal of intercomparability between measurements by different sensors, several of the features used depend implicitly on instrumental and environmental factors. For instance, the frequency is hemmed in by the camera frame rate and the light curve length, which may be limited by observation conditions or operational priorities. Many of the other features can be expected to depend on the sensitivity and noise characteristics of the sensor used – for example, very noisy data will exhibit a lower autocorrelation.

2.2. Uniqueness and Stability

A RSO fingerprint should ideally be both unique, with no two distinct RSOs sharing a fingerprint, and stable, meaning that fingerprints do not change with time – or if they do, only in a predictable manner that still allows an observation to be associated to an object based on its fingerprint.

To quantify uniqueness, following the approach to browser fingerprinting in [11], we consider the surprisal or self-information $I_X(x)$ of the event that the discrete random variable X takes the value x – in our case, that we find the value x for the feature (or the entire fingerprint) X in an observation:

$$I_{\mathrm{X}}(x) = -\log_2\big(p_{\mathrm{X}}(x)\big) \tag{1}$$

Here, $p_X(x)$ is the probability mass function of X. Intuitively, in order to uniquely identify an object x in a population of size $N = |X|$, this sets a target of $I_X(x) \gtrapprox log_2 N$ for the surprisal of the fingerprint derived from a measurement of that object [11].

The entropy $H(X)$ of the distribution is then the expected value of the surprisal:

$$H(X) = -\sum_x p_{\mathrm{X}}(x) \cdot \log_2\big(p_{\mathrm{X}}(x)\big) \tag{2}$$

The entropy of the fingerprint as a whole is equal to the sum of the component's entropies only if the components are statistically independent; otherwise, it is smaller [11]. A design goal for an RSO fingerprint must then be to maximize the fingerprint's entropy by selecting components that are close to statistically independent and have high entropy themselves, but are still feasible to obtain in practice.

As for stability, this property can be assessed either directly, by monitoring the change of the fingerprints or individual fingerprint components derived from measurements of the same object at different times; or by examining the possibility of correctly identifying an RSO from a measurement by associating that measurement's fingerprint of to those of measurements of the same object at different times. In the latter case, a linking mechanism is required to associate fingerprints of measurements at different times. This can be done by a rule-based framework, as has been done for browser fingerprints [11, 12] and as we will demonstrate in this paper by a simple example. It is also a possible application for machine learning and artificial intelligence methods.

It is intuitively apparent that a trade-off exists between uniqueness and stability: A fingerprint shared by all RSOs at all times – i.e. one that is maximally non-unique – is obviously perfectly stable, though not very useful. On the other hand, every object's fingerprint being unique is of limited use if they are not stable, precluding later identification of an RSO by its fingerprint. We also note that perfect uniqueness on the domain of all RSOs is not realistically achievable, at least based on photometric data alone. There are many classes of RSOs whose members are physically practically identically; in fact, due to the prevalence of mega-constellations comprising thousands of satellites, a large part of the RSO population are part of one such class.

3. LIGHT CURVE DATA

3.1. ART Data

To investigate the behaviour of the features and composite fingerprint described above, we recorded light curves of a diverse set of RSOs using the Airbus Robotic Telescope (ART). ART is a passive optical telescope with an aperture of 40 cm, equipped with a modern CMOS camera and a set of photometric Johnson-Cousins filters. Located in Extremadura, southern Spain, ART profits from a dark and clear sky ART achieves a photometric performance of 0.05 mag RMS on fast LEO targets in the Johnson V band [16]. Additionally, ART is capable of producing sub-arcsecond astrometry of RSOs. However, in light curve observation usually only very rough astrometry at the 20 arcsecond level is recorded, mostly for the purposes of airmass correction and recording of the observational geometry.

The observations used in this work encompass 1262 light curves acquired between June and December 2024. 142 different RSOs were observed, with the most-observed object (NORAD cat ID 42907) yielding 39 separate light curves, while others were only observed once - be it for reasons of weather, geometry or prioritization. The observations include all sorts of objects from active satellites to rocket stages and debris, in orbits from LEO all the way to beyond GEO, the most distant observed objects being the Indian Chandrayaan-3 propulsion module (NORAD cat ID 57770) and ESA's recently-retired gamma ray observatory INTEGRAL (NORAD cat ID 27540). Most of the light curves were taken in V, though some were also recorded in Johnson B. A single target is usually observed for 10 to 30 min, adapting the exposure time to the expected brightness of the RSO based on its range. Two example light curves are presented in Fig. 1. Showing a faint – i.e. far – rocket body rotating moderately quickly and a commercial LEO satellite, they exemplify the diversity in RSOs and their lightcurves as well as the range of image frequencies and target magnitudes in ART photometric observations.

3.2. Simulations

We complement the real-world data obtained by ART with a set of synthetic light curves generated by the sensor simulation functionality of SPOOK, an in-house SSA software suite developed by Airbus Defence and Space Germany [18]. This serves a dual purpose: First and foremost, despite its favourable location and extensive automation, ART is subject to the meteorological, operational and technical constraints that affect all ground-based optical telescopes. In particular, the past autumn and winter were unusually poor in nights suitable for photometry. Simulations do not suffer these drawbacks; it is easily possible to obtain a series of observations spanning an extended length of time without interruptions except those imposed by geometry. This is useful to assess the mid– to long-term evolution and stability of RSO fingerprints described in Sec. 2. Second, simulations allow us to easily and quickly explore observing different objects in various physical, orbital and attitude states This lets us develop an intuition for the light curves arising from these different conditions and their respective fingerprints.

For this reason, we decided to simulate long series of observations of only nine fictional objects, each designed to be representative of a class of RSO regularly observed by ART. Fig. 2 shows the simple shape models used in the simulation. We chose four rocket bodies (one each in GTO and MEO, two in LEO) rotating at different rates, three winged cuboid (one tumbling in GEO, one three-axis stabilized each in GEO and LEO) and two cube shapes (one holding its attitude in high MEO, one tumbling in low LEO).

Apart from the absence of inclement weather and other issues exclusive to the real world, the simulations were as close to the real ART's observational programme as possible. We simulated one observation of up to 20 min per object and night for the six-month period from June 1st to November 30th 2024, generating light curves (see Fig. 3) and angle data. This resulted in a total of 1481 light curves. It is worth stressing that this small population of fictional RSOs are not at all intended to be a quantitatively representative sample of the real RSO population. Rather, they are intended to provide a set of observations that is both easily fingerprinted - being a small set of very diverse objects with abundant data available - and chronologically complete in order to investigate the stability of RSO fingerprints. A larger, more representative set of simulated objects might provide interesting insights into the statistics of RSO fingerprint uniqueness that would be hard to replicate using real-world data from a single telescope. However, setting up such a representative population is not a trivial task and was therefore not pursued for this work. The synthetic lightcurves were processed separately from, but otherwise in the same manner as the real-world measurements.

4. RESULTS AND DISCUSSION

4.1. Uniqueness

We extracted the features of Tab. 1 from both the real and synthetic light curves, obtaining a seven-element vec-

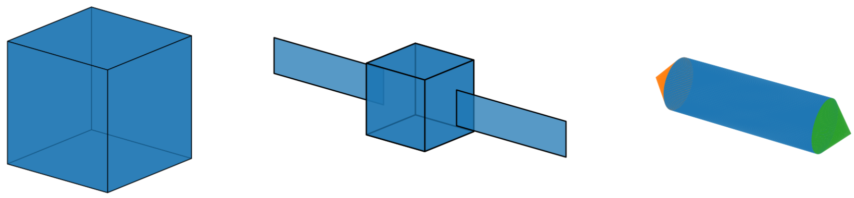

(a) (b) (c)

Figure 2: Object shape models used for the simulations in this work (not to scale): a) cube; b) winged cuboid with specularly reflecting solar panels; c) cylindrical rocket body based on the shape used by Wetterer et al. [1] and Vallverdú Cabrera et al. [17].

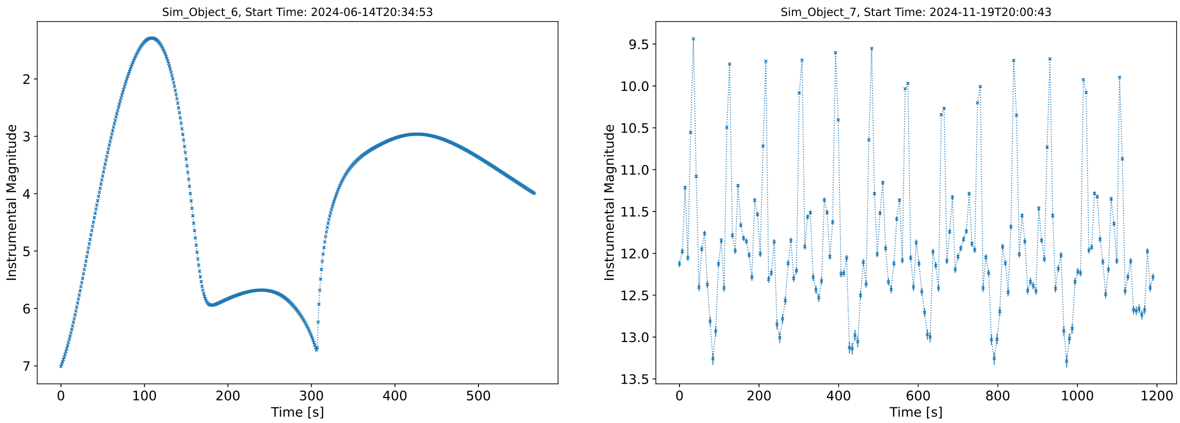

Figure 3: Simulated light curves chosen from the set used for this work. Left: Three-axis controlled winged cuboid in LEO; right: tumbling rocket body in GTO.

Feature	Entropy [bits]
Angular velocity	2.6
Mean magnitude	1.6
Difference of means	1.3
Interpercentile range	1.7
Autocorrelation	1.5
Amplitude	2.0
Frequency	1.1
Total fingerprint	6.6

Table 2: Entropy of the individual features and the fingerprint as a whole.

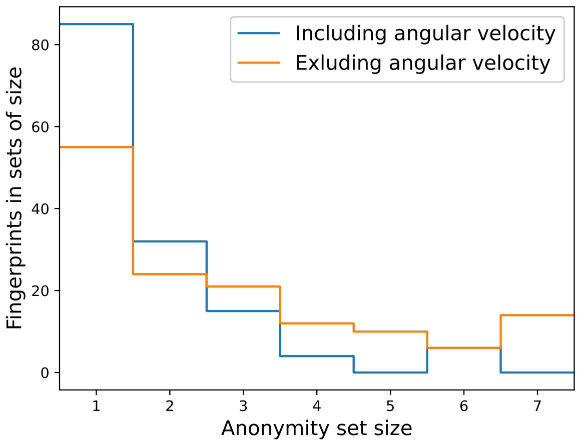

Figure 4: Observed frequency distribution of fingerprints: when including the angular velocity feature as a fingerprint component, 85 fingerprints (out of 142 observed RSOs) are unique

tor of features – or rather feature bin numbers – for each observation. For instance, the fingerprint of an observation of the Starlink satellite with the NORAD catalogue ID 58231 on 2024/07/19 is (6,1,1,1,4,0,0)[1]. To assess the uniqueness of these fingerprints among our set of observed RSOs, we first consider only the first observation of each distinct object. This is to avoid counting objects multiple times, as we are now interested in the uniqueness of the fingerprints among the objects, not among the observations. Using Eq. 2, we can now calculate the entropy of each component feature and the composite fingerprint as a whole. The results are summarized in Tab. 2.

The entropy of the fingerprint as a whole is 6.6 bits, not too far below the $log_2(142) = 7.2$ bit theoretically required to uniquely identify every object in the set. Indeed, by plotting the number of fingerprints whose anonymity set is of size n – i.e. fingerprints which occured n times in our sample – against n (Fig. 4), we can confirm that 85 out of our 142 objects possess unique fingerprints, with a further 32 whose anonymity set is of size 2. The least unique fingerprint in our sample occurs six times, being shared by a mix of GPS and Glonass satellites. The next largest anonymity sets similarly contain different starlink satellites. We notice that the angular velocity, a non-photometric feature, is the feature with the highest entropy on its own. Fig. 4 also shows the case of excluding the angular velocity and limiting the fingerprint purely to photometric measurements, indeed confirming that such a non-photometric component can be a worthwhile addition to the fingerprint. The low entropy of the frequency component may seem surprising at first, but is explained simply by the fact that the majority of RSOs in our sample do not exhibit any periodicity on the timescale of our light curve observations and therefore get sorted into the same frequency feature bin. On the other hand, there is little surprise in the fact that in the simulated set of objects, all fingerprints are unique - a result of the deliberate choice of a small number of very diverse objects.

We therefore conclude that in our sample, the fingerprints as described in Sec. 2 are quite close to being unique. However, it should be noted that this statement does not necessarily transfer to other samples of the RSO population. In particular, it is apparent that much larger samples – up to the entire population – would require the addition of more fingerprint components. Even then, as seen in the example of the six GNSS satellites mentioned above, the method can obviously not be expected to be able to distinguish very similar or even identical objects.

4.2. Stability

A unique fingerprint may still be of little use if does not allow for identification of the object in question, e.g. because it changes over time. To investigate the composite photometric fingerprint's utility in identifying observed objects based on previously recorded fingerprints, we united observations of objects of the same type (e.g. Starlink V2-mini, SL-16 rocket bodies, etc.) into classes, resulting in 48 distinct classes for the real data and nine – one for each object – for the simulations. Next, we need a distance measure between fingerprints, opting for the simple taxicab distance – i.e. the sum of the absolute differences between fingerprint components:

$$d(p, q) = \sum_{i}^{n} |p_i - q_i| \tag{3}$$

We then attempted identification by a very simple algorithm: choose the fingerprint(s) out of the rest of the data which minimize the distance to the fingerprint under consideration. If more than one was chosen, pick one of them randomly. The class of the picked fingerprint is the predicted class of the fingerprint under consideration.

Applying this identification algorithm to all observations in the simulated dataset yields the confusion matrix

[1] Indicating, in order: high angular velocity, bright magnitude, some asymmetry, a moderate change in brightness, high autocorrelation (i.e. a smooth lightcurve), moderate change between subsequent measurements and no periodicity - altogether fairly unsurprising.

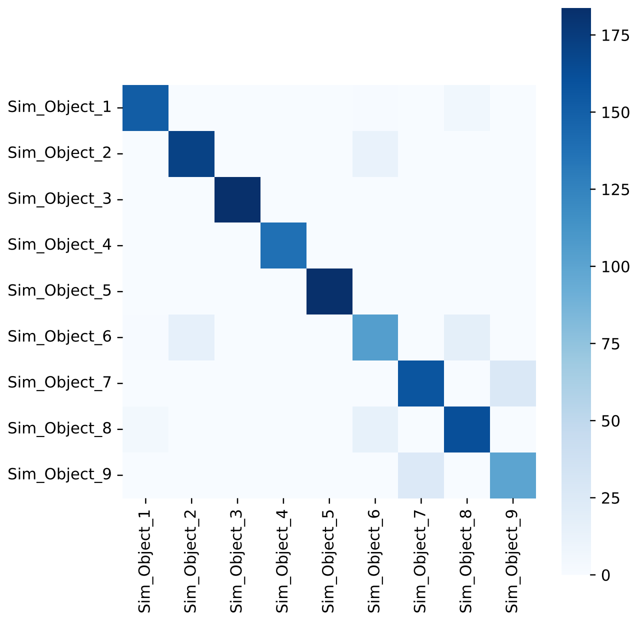

Figure 5: Confusion matrix of object identification by fingerprint in the simulation dataset

shown in Fig. 5. The labels on the left are the true object class, while those on the bottom are the predicted classes; therefore, correct predictions are located on the matrix diagonal, while off-diagonal elements represent misidentifications. Once again, the small number of very different object in the simulated data and large number of observations per class, along with the absence of clouds and similar factors make identification easy. Repeating the same on the real-world data produces the result shown in Fig. 9. Here, we see a larger number of misidentifications. However, many of them are between fairly similar objects. This also highlights that the identification performance is of course dependent on the selection of the classes, with coarser classes tending to enable more reliable, but perhaps less useful, identification. It is also worth noting that for those classes that contain only one observation, identification in this way is impossible.

Finally, we investigated the stability of the fingerprints over time by comparing the distance (Eq. 3) between the fingerprints of observations in the same class to the length of time between the observations. The result for the ART data is shown in Fig. 6. First, it is apparent that, even for observations in very close temporal proximity, the average distance between fingerprints of observations in the same class is considerably larger than the value of zero that would indicate equality of the fingerprints. However, the minimum distance in each bin is zero and continues to be so up to time differences of almost two months. Considering our simple identification algorithm described above, this minimum distance is the more important factor in identification, and one might expect the fingerprint's utility in identifying observations of the same class to decrease after about 60 days in our scenario.

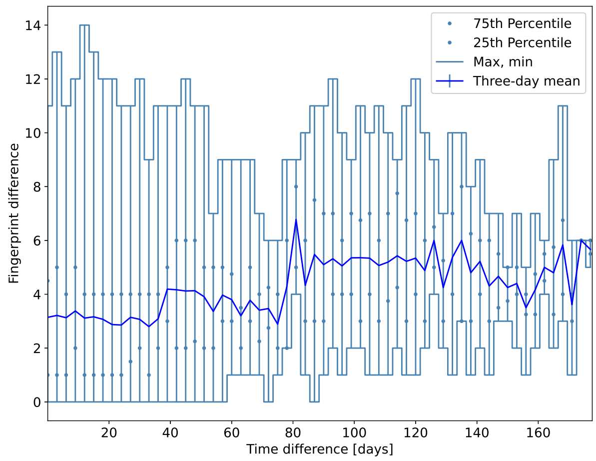

Figure 6: Distance between fingerprints of objects from the same class depending on the time difference between the measurements, including quartiles, minimum and maximum for each three-day bin in time difference.

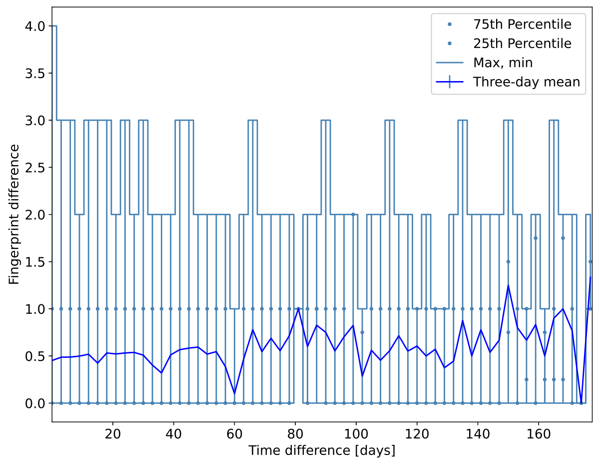

Figure 7: As Fig. 6, but for only the `autocorrelation` feature.

Creating the same plot for single components of the fingerprint does not reveal any obvious time dependencies. For the sake of conserving space, only the plot for the autocorrelation component is shown here(Fig. 7).

For the simulated light curves, the same is shown in Fig. 8. In accordance with the results of the identification test above, in the simulated data set the minimum fingerprint distance stays at zero for all time differences, enabling identification. Also of note in this figure is the slight arch of the average distance curve, slightly rising and then falling again. This might be related to seasonal effects due to the changing observation and illumination geometry.

We conclude that the composite photometric fingerprint, in the form and with the components described here, is stable at least on the scale of weeks to months, in the sense of its utility for identification.

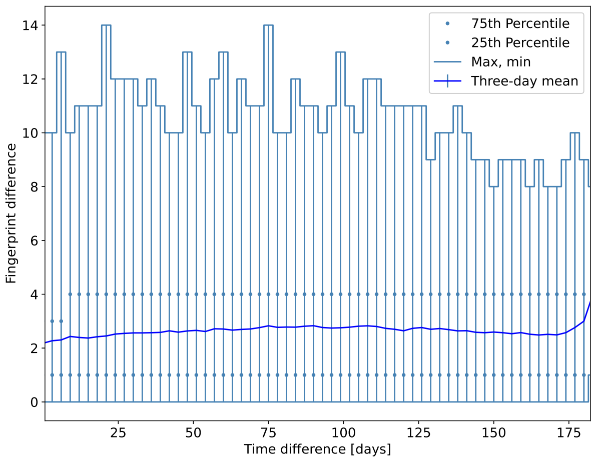

Figure 8: As Fig. 6, but for the simulated light curves.

5. OUTLOOK AND SUMMARY

In this paper, the concept of a composite RSO fingerprint made up of photometric and other features was described, implemented and first tests conducted. We selected seven features to comprise our fingerprint and extracted fingerprints from two sets of RSO light curve data, one simulated and the other created from real-world observations of the Airbus Robotic Telescope (ART).

We found that most of the objects in our real-world sample have a unique fingerprint, with many of those that do not sharing theirs with objects of the same or very similar types. However, we caution that larger sets of RSOs may require the augmentation of the fingerprint with additional features. We also attempted to classify which RSO produced a light curve based on the fingerprint derived from the light curve. This was highly successful in the very fingerprintable simulation dataset, while the real data suffered from a higher number of misidentifications. However, most of these were again between fairly similar objects, highlighting the fundamental inability of photometry-based methods in distinguishing between physically highly similar objects. Lastly, we investigated the change of the fingerprints over time. We found that the average distance between fingerprints of the same object is already surprisingly large even for observations in close temporal proximity. However, it does not rise quickly with the time difference between observations, showing a marked increase only after almost two months.

While these initial results are promising, showing that even a fingerprint consisting of relatively few very simple features can aid in distinguishing between and identifying RSOs, there are certain improvements that should be investigated, both in the selection of fingerprint components and the linking of fingerprints from different observations. Not only is there a multitude of features that were not considered in this work, but the very crude binning of feature values performed in this work could be compared to more sophisticated approaches. Similarly, the simple fingerprint linking by minimal taxicab distance could like be improved. The application of modern modern machine learning approaches to both tasks appears an enticing prospect. Additionally, the application to a larger set of light curves is planned.

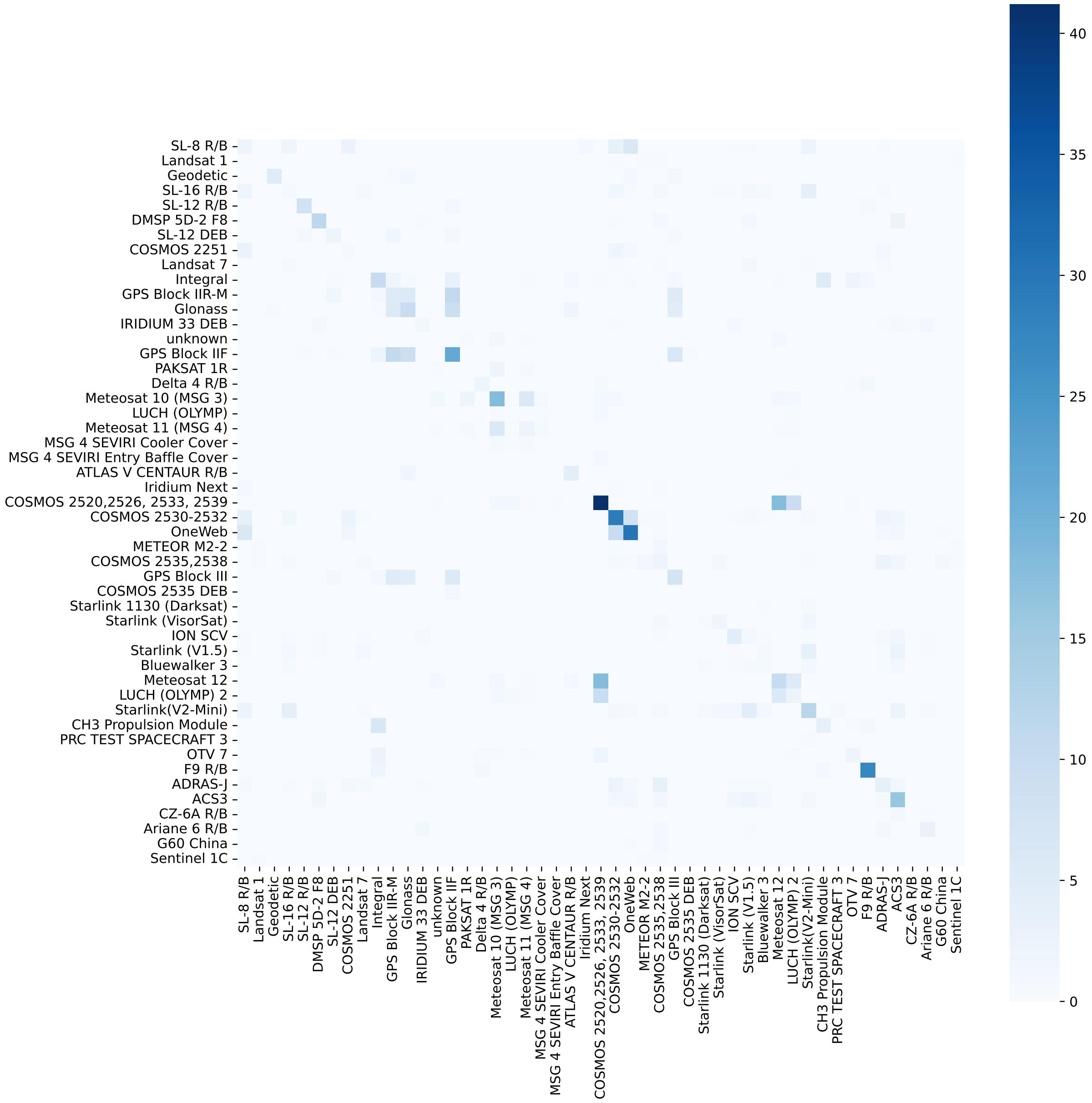

Figure 9: Confusion matrix for object identification by closest fingerprint in the ART data. While there are many misidentifications, they often occur between very similar objects (e.g. GPS Block IIR/F and Glonass in the top right).

REFERENCES

1. Wetterer, C. J. and Jah, M. (2009). "Attitude Determination from Light Curves". *Journal of Guidance, Control, and Dynamics* 32.5, pp. 1648–1651. DOI: 10.2514/1.44254.
2. Vasile, M. et al. (2024). "Space object identification and classification from hyperspectral material analysis". *Scientific Reports* 14.1, p. 1570. DOI: 10.1038/s41598-024-51659-7.
3. Schildknecht, T. et al. (Jan. 2009). "Reflectance Spectra of Space Debris in GEO". *Advanced Maui Optical and Space Surveillance Technologies Conference*. Ed. by S. Ryan.
4. Zigo, M. (2019). "BVRI Photometry of Space Debris Objects at the Astronomical and Geophysical Observatory in Modra". AMOS, Advanced Maui Optical and Space Surveillance Technologies Conference, p. 8.
5. Friedman, A. M. and Frueh, C. (Apr. 2022). "Observability of Light Curve Inversion for Shape and Feature Determination Exemplified by a Case Analysis". *The Journal of the Astronautical Sciences* 69.2, pp. 537–569. DOI: 10.1007/s40295-021-00293-w.
6. Olson, T. et al. (2024). "ML-Based Photometric Fingerprinting at Scale for LEO Satellite Monitoring". AMOS, Advanced Maui Optical and Space Surveillance Technologies Conference.
7. Dao, P., Heinrich-Josties, E., and Boroson, T. (2016). "Automated Algorithms to Identify Geostationary Satellites and Detect Mistagging using Concurrent Spatio-Temporal and Brightness Information".
8. Chaudhary, A. B. et al. (2011). "Fingerprinting of Non-resolved Three-axis Stabilized Space Objects Using a Two-Facet Analytical Model". AMOS, Advanced Maui Optical and Space Surveillance Technologies Conference. Maui, Hawaii.
9. Putman, T. (2024). "Multi-Phenomenology Fusion for Satellite Identification".
10. Cirillo, G. et al. (2023). "AIRBUS ROBOTIC TELESCOPE AND SPOOK AS TEST-BED FOR SPACE-BASED SPACE SURVEILLANCE". *Proc. 2nd NEO and Debris Detection Conference*. 2nd NEO and Debris Detection Conference. Darmstadt: ESA Space Safety Programme Office.
11. Eckersley, P. (2010). "How Unique Is Your Web Browser?" *Privacy Enhancing Technologies*. Ed. by M. J. Atallah and N. J. Hopper, pp. 1–18. DOI: 10.1007/978-3-642-14527-8_1.
12. Pugliese, G. et al. (2020). "Long-Term Observation on Browser Fingerprinting: Users' Trackability and Perspective". *Proceedings on Privacy Enhancing Technologies* 2020.2, pp. 558–577. DOI: 10.2478/popets-2020-0041.
13. Richards, J. W. et al. (2011). "ON MACHINE-LEARNED CLASSIFICATION OF VARIABLE STARS WITH SPARSE AND NOISY TIME-SERIES DATA". *The Astrophysical Journal* 733.1, p. 10. DOI: 10.1088/0004-637X/733/1/10.
14. Orwat-Kapola, J. K. et al. (2021). "Light-curve fingerprints: an automated approach to the extraction of X-ray variability patterns with feature aggregation – an example application to GRS 1915+105". *Monthly Notices of the Royal Astronomical Society* 509.1, pp. 1269–1290. DOI: 10.1093/mnras/stab3043.
15. VanderPlas, J. T. (May 2018). "Understanding the Lomb-Scargle Periodogram". *Astrophysical Journal Supplement Series* 236.1, 16, p. 16. DOI: 10.3847/1538-4365/aab766.
16. Kuhn, M. and Dekorsy, T. (2024). "Persistent Signatures for Space Object Fingerprinting". IAC. Milan.
17. Vallverdú Cabrera, D., Utzmann, J., and Förstner, R. (2022). "The adaptive Gaussian mixtures unscented Kalman filter for attitude determination using light curves". *Advances in Space Research*. DOI: 10.1016/j.asr.2022.11.027.
18. Vallverdú Cabrera, D. et al. (2021). "INTEGRATION OF ATTITUDE CHARACTERIZATION IN A SPACE DEBRIS CATALOGUE USING LIGHT CURVES". 8th European Conference on Space Debris (virtual). Darmstadt, Germany, p. 13.